

RESEARCH

Open Access



# The Shear Capacity Estimation of Reinforced Concrete Short Beams with Steel Fiber by Digital Image Correlation Approach

Narawit Hemstapat<sup>1\*</sup>, Kazumasa Okubo<sup>1</sup>, Junichiro Niwa<sup>1</sup> and Mitsuyasu Iwanami<sup>1\*</sup>

## Abstract

This research aimed to estimate the shear capacity of reinforced concrete short beams with steel fiber (RSF short beams) using DIC (digital image correlation). Four-point bending tests of RSF short beams with shear span ratio ( $a/d$ ) of 1.0, 1.5, and 2.0 were conducted. 0.5% or 1.0% volume fraction of steel fiber was used. The distribution of minimum principal strain ( $\epsilon_2$ ) was obtained from DIC then the width of compressive strut was evaluated. The effects of volume fraction of steel fiber and shear span ratio were investigated. Finally, the shear capacity of RSF short beams was estimated with the help of DIC.

**Keywords** Compressive strut, DIC, Short beam, Steel fiber, Shear

## 1 Introduction

Steel fiber reinforced concrete (SFRC) is a concrete, where steel fiber was added. The benefit of steel fiber includes shear reinforcement, blast-resistant, precast, slope stabilization, repairs, etc. (Banthia & Trottier, 1994). The steel fiber can improve the concrete abrasive resistance (Mansouri et al., 2020). It also plays a role in determining the failure mode of reinforced concrete beams with steel fiber (RSF beams) after fire (Antonius et al., 2020). Moreover, it can be recycled for a more environmentally friendly application (Qin & Kaewunruen, 2022). In addition, it will act as crack arrestors similar to that of aggregates (Swamy & Mangat, 1974). This will increase the tensile resistance of concrete by controlling crack opening. The ductility will increase significantly,

since steel fiber will continue to transfer forces across the cracks (Marti et al., 1999). The addition of steel fiber increases the shear capacity and tends to change the failure mode from brittle to ductile (Khuntia et al., 1999). Furthermore, there were also applications with other materials, for example, an ultra-high-performance fibre-reinforced concrete (UHPFRC) made with hybrid fibers (steel and polypropylene) (Nuaklong et al., 2020).

For the shear failure of reinforced concrete (RC) beams, there are four failure modes called diagonal tension, shearing, shear compression, and web crushing (Placas & Regan, 1971). To estimate the shear capacity of RC beams, most codes of practice use semi-empirical relations based on the available experimental results (Tan et al., 1993). It has been shown that the randomly dispersed and oriented steel fibers in concrete can enhance the mechanical properties of RC beams (Birincioglu et al., 2022).

There are beam action and arch action in the shear resisting mechanisms of RC beams (Gunawan et al., 2020). In the case of RC short beams, the final failure will be caused by a dowel failure or crushing of the compression zone (shear compression) (MacGregor, 1997). In such a case, the arch action is dominant, the compressive

Journal information: ISSN 1976-0485/eISSN 2234-1315

\*Correspondence:

Narawit Hemstapat  
narawit.hem@gmail.com  
Mitsuyasu Iwanami  
iwanami@cv.titech.ac.jp

<sup>1</sup> Department of Civil and Environmental Engineering, Tokyo Institute of Technology, 2-12-1 Ookayama, Meguro-Ku, Tokyo 152-8552, Japan

strut is the important component for the estimation of the shear capacity. By being able to calculate the compression force in the compressive strut, it is considered that the shear capacity can be estimated. The compression force can be calculated using the width of compressive strut and the compressive stress occurring in the strut.

Digital image correlation (DIC) can capture the displacement distribution that occurs on the surface of the object. It is able to memorize the pattern of the black and white on the object at the original stage in the photo image. The pattern can change after the object is deformed and DIC can analyze the differences between the changed pattern and the original pattern. Then, the strain can be calculated with the displacement field that contains displacements at many points in the object. For the preparation of DIC applied to the loading test of RC beams, the surface of beam specimens must be sprayed in black and white to create an original pattern for the analysis.

Normally, the image analysis and DIC were used to find the crack width and strain distribution. Their previous researches in the structural concrete field are summarized below.

Jongvitsakul et al. (2011) applied the image analysis (using the grid of colored stickers as a pattern on the concrete surface) to obtain the crack width in RSF slender beams ( $a/d=2.8$ ) and proposed the prediction method for the shear capacity. Lee et al. (2019) used the image analysis to investigate the cracking and fracture stages in RC beams. Moreover, Zarrinpour and Chao (2017) used DIC to investigate the crack width and strain distribution to calculate the contributions of compression zone, bridging effect, and dowel action in detail to the shear capacity of RSF slender beams. There was also an application of DIC to monitor the diagonal crack width in high strength (around 60–65 MPa) RC and RSF short beams. The results showed that the steel fiber delayed the appearance of the diagonal crack (Tahenni et al., 2016). DIC was used for the crack propagation analysis, such as crack width and strain contours in synthetic, steel, hybrid fiber reinforced concrete beams (Bhosale & Prakash, 2020). DIC for crack measurement of RC beams can be verified by comparing the visual and DIC results (Destrebecq et al., 2011). Furthermore, there was a combination of fiber-optic sensors and DIC for damage detection, localization in structural health monitoring (Morgese et al., 2021).

However, in the case of RSF short beams, the method to estimate the width of compressive strut has not been developed so far. This research attempted to estimate the shear capacity of RSF short beams. To achieve this, the focus of this research is the compressive strut which is the main contribution in the shear capacity of RSF short

beams. If the force in the compressive strut can be calculated, the shear capacity can be estimated. The force in the compressive strut is strongly related to the width of the compressive strut and the compressive stress. The compressive stress can be calculated using the compressive strength, while the width of compressive strut needs to be investigated.

Therefore, the objective of this study is to estimate the shear capacity of RSF short beams by investigating the width of compressive strut using DIC. The aim is to capture the contribution of compressive strut directly for the shear capacity of RSF short beams. To achieve this, DIC will be used to observe the minimum principal strain ( $\epsilon_2$ ) for the estimation of the width of compressive strut.

## 2 DIC-Based Evaluation of the Width of Compressive Strut for Shear

To estimate the shear capacity of RSF short beams accurately, the estimation method should be based on the experimental data. Fig. 1 shows the free-body diagram of a RSF short beam. From Fig. 1, the shear capacity can be calculated by focusing on the compressive strut. The strut can be treated as a concrete prism embedded in the shear span, where the compression force acts dominantly. The compression force in the compressive strut can be calculated using the concrete compressive stress and width of compressive strut.

This research investigated this compressive strut using DIC. The distribution of minimum principal strain ( $\epsilon_2$ ) was obtained from DIC in the shear span of RSF short beams.  $\epsilon_2$  is defined as the minimum normal strain that occurs in the beam.  $\epsilon_2$  is assumed to generate in the compressive strut in the same direction as the strut. The distribution of  $\epsilon_2$  in the direction perpendicular to the compressive strut along the representative line was investigated for estimating the width of compressive strut. The gage length of 30 mm was used as the original length of the displacement fields in the shear span for the calculation of  $\epsilon_2$  by DIC. To calculate the  $\epsilon_2$  at one point, all the data of displacements 15 mm away from the point were used, as shown in Fig. 2. Therefore, the zone of at least 15 mm away from the edges of target region of DIC was neglected due to the insufficiency of data. The region of interest is the area of the test shear span. The  $30 \times 30$  mm area at left top corner is an example of the gage length used for calculation of the minimum principal strain at one point of the center of  $30 \times 30$  mm area.

## 3 Experimental Program

### 3.1 Experimental Outlines

Four-point bending tests of six RSF short beams were conducted. The parameters were volume fraction of

steel fiber and shear span ratio ( $a/d$ ). The experimental cases are shown in Table 1 and the details of beams are shown in Fig. 3.

### 3.2 Materials and Mix Proportions

5D steel fibers were used for the mix. The properties are shown in Table 2. The mix proportions are shown in Table 3. Deformed bars were used for the tensile reinforcements, compression reinforcements, and stirrups. The details are shown in Table 4.

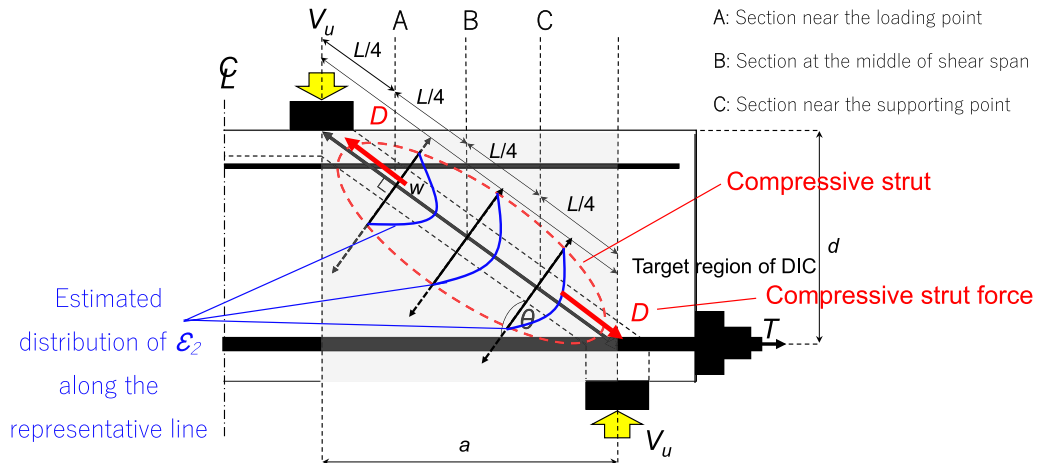


**Fig. 1** Outline for finding the width of the compressive strut

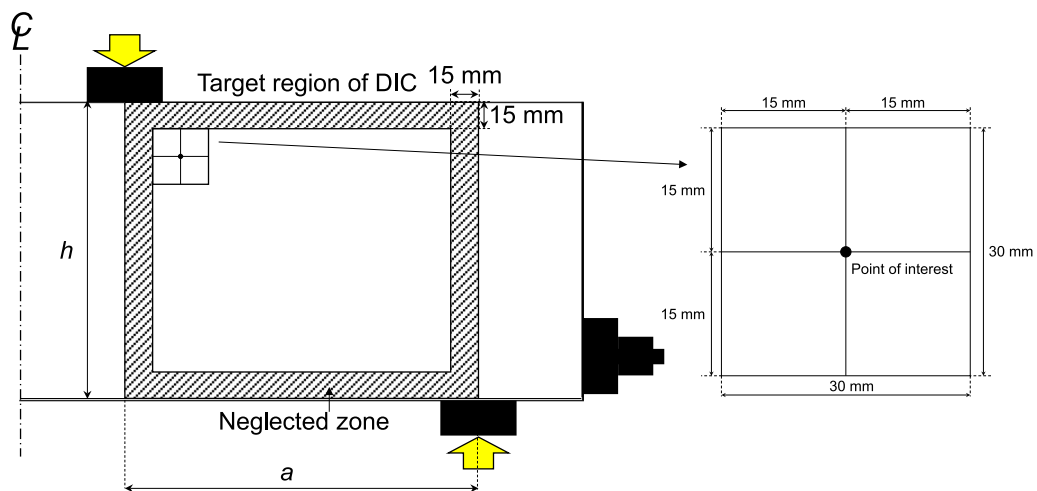


**Fig. 2** Range of data for calculation of  $\epsilon_2$

**Table 1** Experimental cases of RSF short beams

No.	Name	Volume fraction (%)	Design compressive strength (MPa)	Shear span ratio, $a/d$	No. of specimens
1	N0.5F-1.0	0.5	40.0	1.0	1
2	N0.5F-1.5			1.5	1
3	N0.5F-2.0			2.0	1
4	N1.0F-1.0	1.0		1.0	1
5	N1.0F-1.5			1.5	1
6	N1.0F-2.0			2.0	1

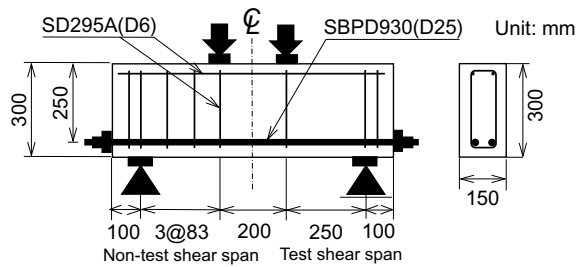


**Fig. 3** Details of a beam with shear span ratio of 1.0

### 3.3 Specimens

The beams were designed with an effective depth of 250 mm. The shear span ratios were 1.0, 1.5, 2.0 varied by the shear span length of 250, 375, 500 mm, respectively. The cross-sectional dimensions were identical, 150 × 300 mm. The tensile reinforcement ratio was 2.7%. Each beam was divided into the test shear span and the non-test shear span. The beams were asymmetrically designed to fail in the test shear span. The test shear span was not reinforced with any stirrups, while the non-test shear span was reinforced with stirrups to prevent the shear failure. The four-point bending was applied to the beams. The external load was distributed evenly. The shear stress distribution should be even. This asymmetric stirrup arrangement may have an uneven effect on the effectiveness of the concrete, stirrup, and steel fibers. However, it is believed that the uneven effect would be slight. This asymmetric arrangement is intended to control the shear span to failure for the DIC. In fact, it is relatively commonly used in this research area, and Jongvivatsakul et. al. (2011) and Zarrinpour and Chao (2017) have experimented with this technique.

**Table 2** Properties of 5D steel fiber

Type	Length ( <i>l</i> ) (mm)	Diameter ( <i>d</i> ) (mm)	Aspect ratio ( <i>l/d</i> )	Tensile strength (MPa)	Density (kg/m <sup>3</sup> )	Elastic modulus (GPa)	End shape
5D	60	0.90	66.7	2300	7850	210	

**Table 3** Mix proportions

Mix	$f'_c$ (MPa)	Volume fraction (%)	W/C (%)	<i>s/a</i> (%)	Density (g/cm <sup>3</sup> )		Unit weight (kg/m <sup>3</sup> )				
					S	G	W	C	S	G	SP
A	40.0	0.5	50	50	2.45	2.65	175	350	821	885	0.6% C
B		1.0					175	350	821	885	1.3% C

Specimens with mix proportion:

A: N0.5F-1.0, N0.5F-1.5, N0.5F-2.0

B: N1.0F-1.0, N1.0F-1.5, N1.0F-2.0

$f'_c$ : concrete compressive strength; *s/a*: volume ratio of sand to aggregate; W: water; C: high-early-strength Portland cement; S: sand; G: coarse aggregate (20 mm maximum size) and SP: superplasticizer

**Table 4** Details of reinforcements

Type	Nominal diameter (mm)	Yield strength (nominal/actual) (MPa)
Compressive	6.35	295/312
Stirrup	6.35	295/312
Tensile	25.0	930/1002

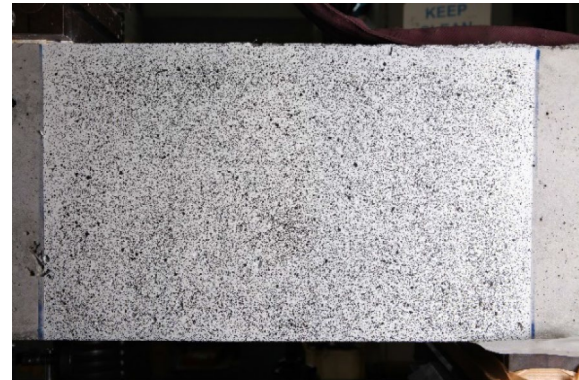


**Fig. 4** Sprayed test shear span of N1.0F-2.0 beam

### 3.4 Experimental Procedure

The test shear span of each beam was sprayed in black and white for DIC. Fig. 4 shows the example of the sprayed test shear span. Nuts and anchor plates were provided at the ends of tensile reinforcements to prevent the anchorage failure. Sufficient tensile anchorage was provided by tightening the bolt using a spanner without a specific torque. The loading and supporting plates' widths were 65 and 72 mm, respectively. Teflon

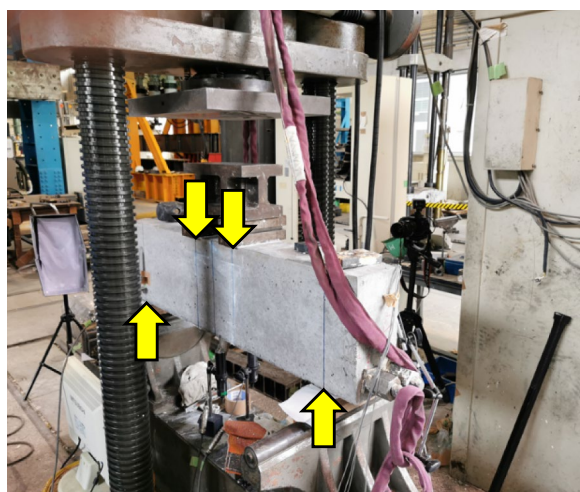


**Fig. 5** Beam subjected to four-point bending

sheets with the silicon grease in between were placed between a beam and supporting plates to eliminate the horizontal friction. Loading plates and a spreader beam were used for the loading. Beams were subjected to four-point bending on simple supports. The loading rate was approximately 10 kN/min. The measurements of load and vertical displacement were done during the tests. The displacement transducers were placed at the mid-span and supports. Photos were taken for the investigation of cracking behavior and for DIC. This research used Canon 5D mark II with EF 24–70 mm lens for a camera, Cineroid LM800V (light angle: 120°, color temperature: 2700–6500 K ± 200 K, photometric with brightness: 3400 Lux at 1 m distance) for a light and sDIC program from SEIKA digital image corporation. The camera, light and program were commercial. The example of a test is illustrated in Fig. 5.

## 4 Results and Discussions

### 4.1 Load–Deflection Curve

The load–deflection curves are shown in Figs. 6, 7, and 8. The peak load increased significantly when the volume fraction of steel fiber was increased and the shear span ratio was decreased. The experimental results are summarized in Table 5.

### 4.2 Effects of Volume Fraction of Steel Fiber and Shear Span Ratio

From Figs. 6, 7, and 8 and Table 5, the increase in volume fraction of steel fiber increased the shear capacity by 35%, 23%, and 24% in the shear span ratio of 1.0, 1.5–2.0, respectively. The increase was larger when the shear span ratio was lower.

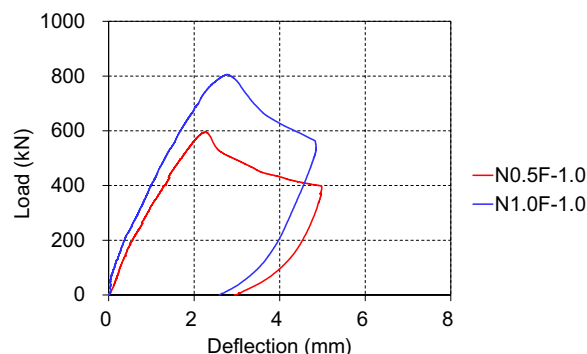


**Fig. 6** Load–deflection curves of RSF short beams with shear span ratio of 1.0

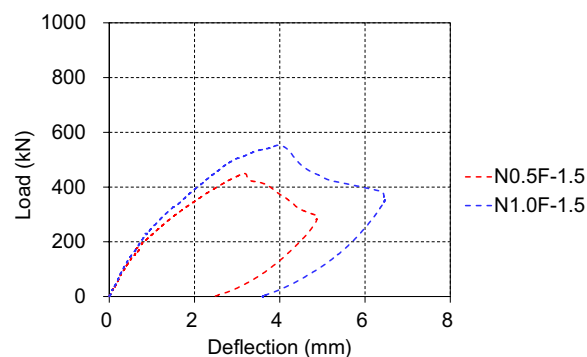


**Fig. 7** Load–deflection curves of RSF short beams with shear span ratio of 1.5

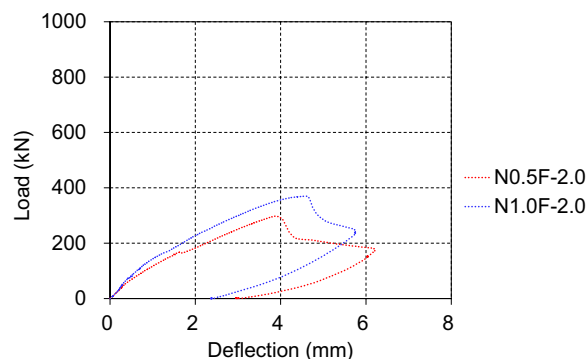


**Fig. 8** Load–deflection curves of RSF short beams with shear span ratio of 2.0

Fiber stresses perpendicular to the crack surfaces are equilibrated by compressive stresses on the crack surfaces, which greatly enhance aggregate interlock (Kaufmann et al., 2019). Therefore, in the low shear span ratio, where the compressive stresses were more

**Table 5** Experimental results of RSF short beams

No	Name	$f'_c$ (MPa)	$a/d$	Peak load (kN)	Deflection at the peak load (mm)	$V_{exp}$ (kN)
1	N0.5F-1.0	41.0	1.0	594.8	2.26	297.4
2	N0.5F-1.5		1.5	449.6	3.17	224.8
3	N0.5F-2.0		2.0	298.0	3.88	149.0
4	N1.0F-1.0	52.5	1.0	805.6	2.78	402.8
5	N1.0F-1.5		1.5	552.4	3.93	276.2
6	N1.0F-2.0		2.0	369.6	4.56	184.8

$f'_c$ : concrete compressive strength;  $a/d$ : shear span ratio;  $V_{exp}$ : experimental shear capacity

dominant on the crack surfaces, the effect became more significant.

With the decrease in shear span ratio from 2.0 to 1.5, the shear capacity increased 51% and 49%, in the case of 0.5% and 1.0% volume fraction of steel fiber, respectively. On the other hand, when the decrease in shear span ratio was from 1.5 to 1.0, the shear capacity increased 32% and 46%, in the case of 0.5% and 1.0% volume fraction of steel fiber, respectively. When the decrease in shear span ratio was from 2.0 to 1.5, the increase in the shear capacity was nearly equal in both volume fractions but higher than that of 1.5 to 1.0. When the decrease in shear span ratio was from 1.5 to 1.0, the increase in the shear capacity was larger in 1.0% volume fraction of steel fiber than that of 0.5% volume fraction of steel fiber. The tests results confirmed the correlation between the volume fraction of steel fiber and the shear span ratio.

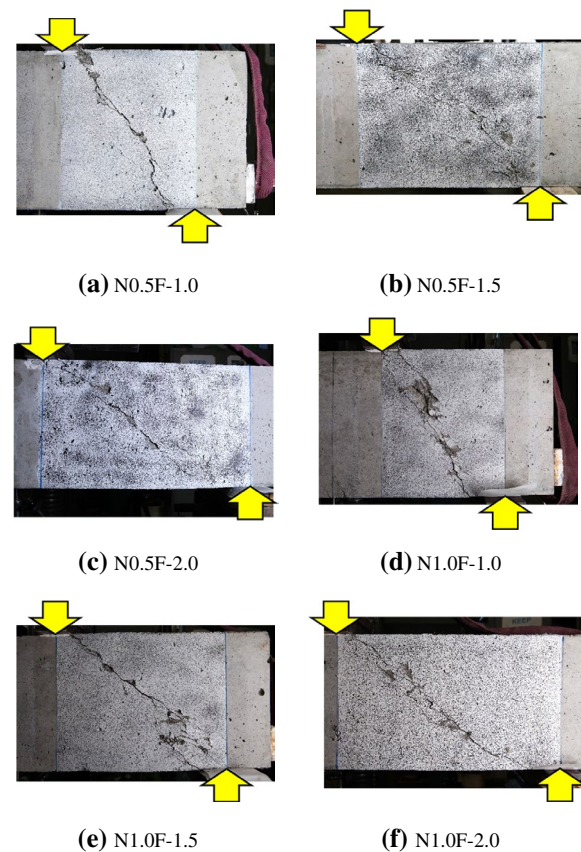
The photos of each beam after the tests are shown in Fig. 9. All the beams show critical diagonal cracks propagated with the local angles changing along the test shear span. However, all the critical diagonal cracks were in between loading and supporting points. The angles of critical diagonal cracks inversely varied with the shear span ratio.

## 5 Width of Compressive Strut obtained from DIC

### 5.1 Determination of the Width of Compressive Strut

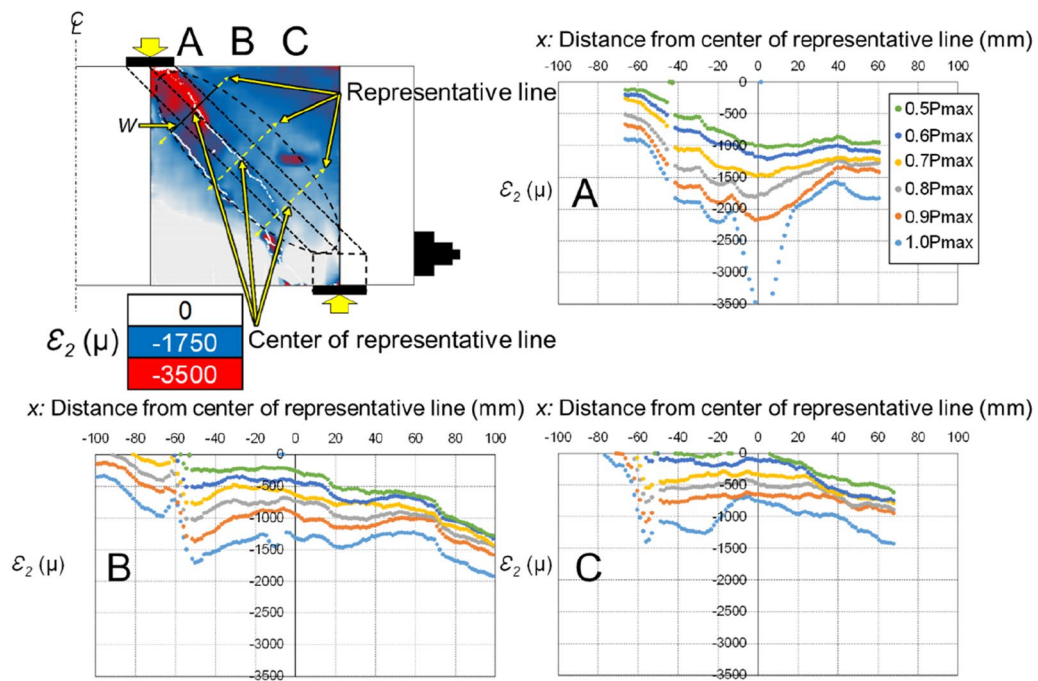
The distribution of minimum principal strain ( $\epsilon_2$ ) at Sections A, B and C in the direction perpendicular to the compressive strut is shown in Fig. 10 which illustrates N0.5F-1.0 and N1.0F-2.0 as the representative. By observing the contour plot of  $\epsilon_2$ , the high-level strain was concentrated between the loading and supporting points, especially near the loading point.

According to MacGregor (1997), a short beam transfers shear forces from loading points to supports by compressive stresses rather than shear stresses. After diagonal cracks extend from the loading points to the supports or the steel unbonded, the shear flow cannot be transmitted. Therefore, the load after the interruption of the shear

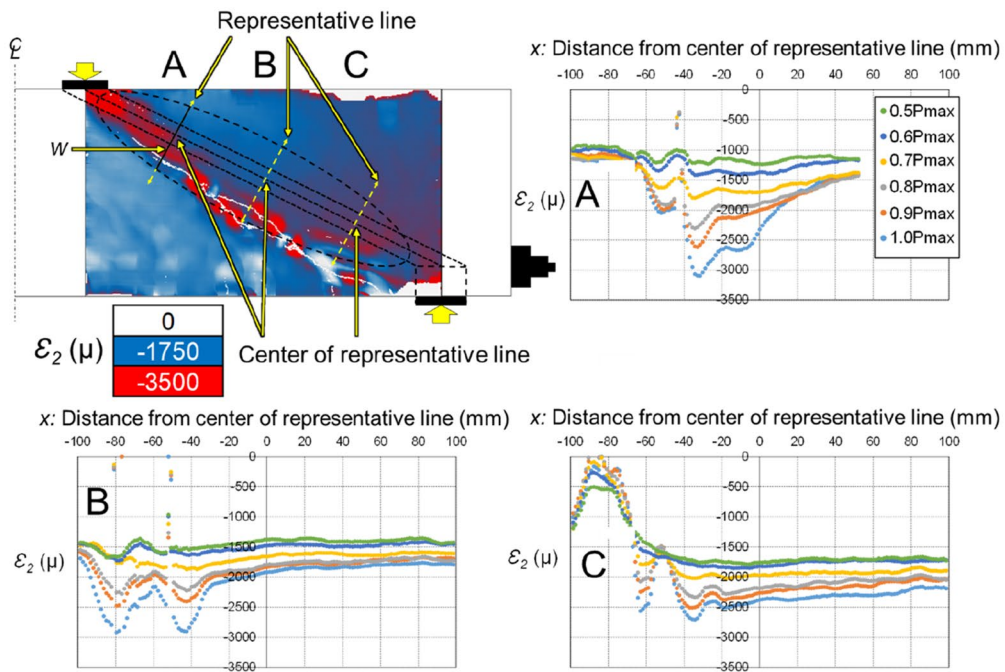
**Fig. 9** Crack patterns of RSF short beams

flow will be carried in part by arch action in a form of compressive strut. The compressive strut represents concrete compressive stress fields.

When there is the compressive strut due to arch action, the compressive stress occurs in the test shear span, causing the concentration of the compressive strain. By investigating the concentration and range of the strain distribution, the compressive strut can be identified.



(a) N0.5F-1.0



(b) N1.0F-2.0

**Fig. 10** Distribution of  $\epsilon_2$  in RSF short beams at the peak load in several regions

To evaluate the shape and size of the compressive strut, the distributions of  $\epsilon_2$  in several regions were investigated. The distribution of  $\epsilon_2$  in the direction perpendicular to the strut at one-fourth, half, three-fourth of the strut length from the loading point [Sections A, B, C (Fig. 1), respectively] was obtained from DIC in the test shear span of RSF short beams, as shown in Fig. 10.

By plotting  $\epsilon_2$  at some load levels, the distribution similar to a parabolic curve can be seen in the region near the loading point (Section A). Regardless of the load level, in the other regions (Sections B and C), the relatively uniform distribution can be seen.

Then, to estimate the width of compressive strut, the  $\epsilon_2$  distribution at the peak load near the loading point (one-fourth of the strut length, Section A) was focused on. As shown in Fig. 11(i), the distribution was approximated by the parabolic curve if the data outside of strut and obvious errors due to the shear crack were ignored, since the sprayed pattern was broken in the closest area to the

shear crack (the zero-strain occurred from the broken pattern was excluded beforehand). Therefore, the results in this area should be ignored.

The approximation of parabolic curve from the selected data is shown in Fig. 11(ii). From the parabolic curve, it is defined that the center of the strut is located at the peak point of the parabolic curve, while the boundary of the strut is located at the zero strain which is the intercept of the parabolic curve.

From this definition, the width will give an unconservative estimation of the shear capacity of RSF short beams. According to MacGregor (1997), there is an idealized prismatic strut or uniformly tapering member. The width often varies, because the concrete at midlength of the strut is wider than at the ends. The strut can be idealized as a bottle-shaped or local truss model.

Since these idealizations of strut might not represent the actual shape of strut, it is preferable to capture the

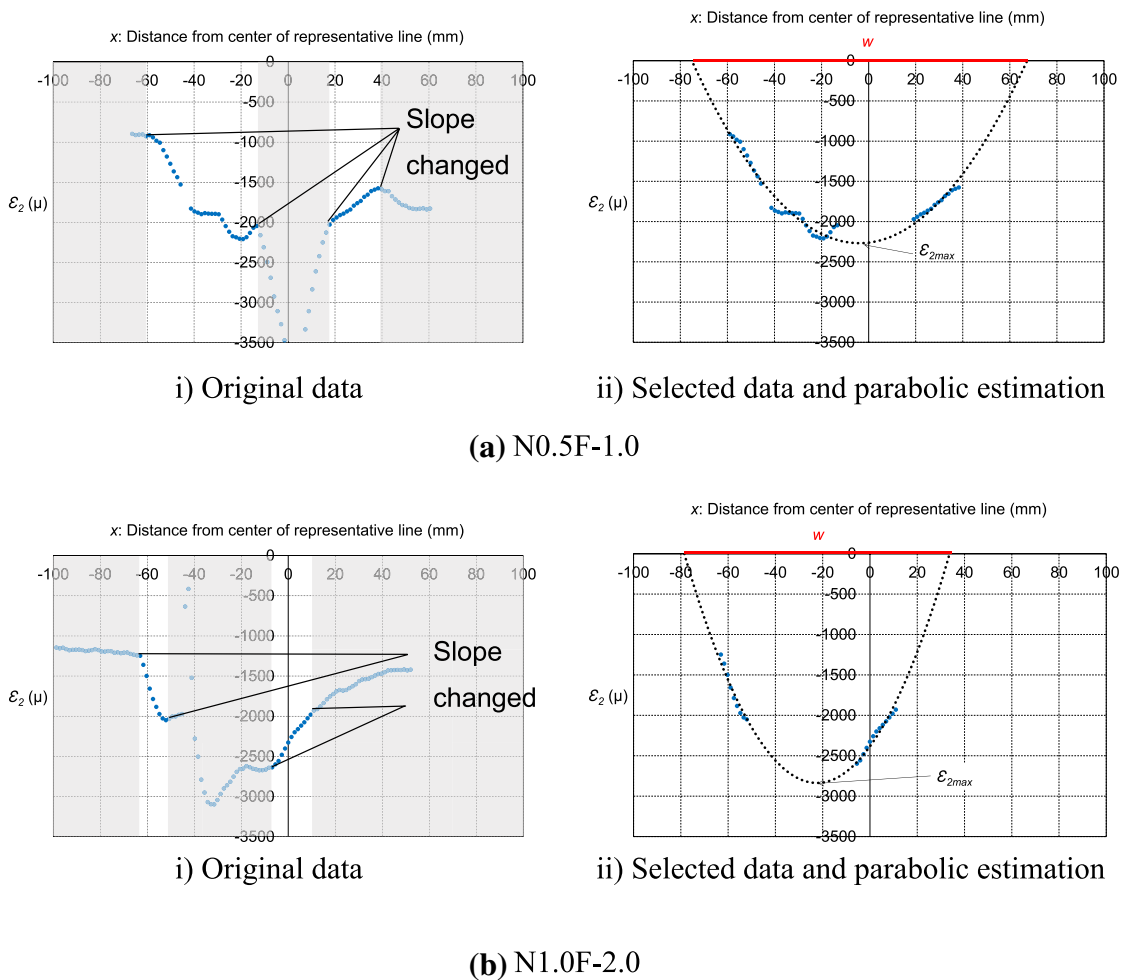


**Fig. 11** Parabolic estimations

strut experimentally, because the results are from the loading test directly. However, it is still difficult to capture the actual shape and width of compressive strut from the experiment. Nevertheless, the width of compressive strut is crucial for the estimation of the shear capacity of RSF short beams.

Therefore, the shape and width of compressive strut in this research was assumed to be uniform for the simple approximation. In addition, the effect of cracked concrete at the peak load will be accounted for in this research. Cracked concrete subjected to high tensile strains in the direction perpendicular to the compression is softer and weaker in compression than concrete in a standard cylinder test (Vecchio & Collins, 1986). The results according to this definition will be discussed later by comparison between the experimental and calculated shear capacity.

## 5.2 Effects of Parameters on the Width of Compressive Strut

According to the estimation results of the width of compressive strut, as shown in Fig. 12, with the increase in the volume fraction of steel fiber, the width increased significantly in beams with the shear span ratio of 1.0 and 1.5. However, the decrease in the width was observed in the shear span ratio of 2.0. It is considered that in the shear span ratio of 1.0 to 1.5, the bridging effect became more notable, while in the shear span ratio of 2.0, the mechanism of the strut (arch action) was not significant.

## 6 Calculation of Shear Capacity Using the Width of Compressive Strut from DIC

In this research, compressive strut and tension tie were assumed to bear only axial forces, as shown in Fig. 1. By considering the equilibrium of vertical forces at the supporting point, Eq. 1 can be obtained. Equation 2 describes the calculation of shear capacity using the force and angle of compressive strut:

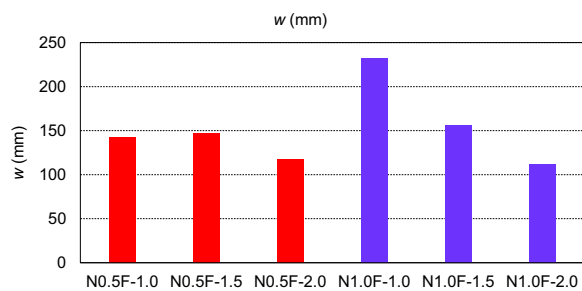


**Fig. 12** Width of compressive strut

$$V_{\text{DIC}} = D \sin \theta, \quad (1)$$

$$V_{\text{DIC}} = f_c' b_w k w \sin \left( \cot^{-1} (a/d) \right), \quad (2)$$

where  $V_{\text{DIC}}$  is the shear capacity calculated from DIC (N),  $D$  is the force in compressive strut,  $\theta$  is the angle of compressive strut,  $b_w$  is the web thickness (mm),  $k$  is the reduction factor regarding the compressive stress in cracked concrete and width of compressive strut at the peak load,  $w$  is the width of compressive strut (mm).

If the full compressive strength and full width of strut were used for the calculation of the shear capacity ( $k=1.00$ ), it will be unconservative. By considering the failure and cracking of concrete at the peak load, cracked concrete at the peak load will not provide the full compressive strength.

According to Vecchio and Collins (1986), cracked concrete subjected to high tensile strains in the direction perpendicular to the compression is softer and weaker in compression than concrete in a standard cylinder test. In addition, in this calculation, the width of compressive strut was determined from the distribution of  $\mathcal{E}_2$  and that the boundary of the strut was defined as where the  $\mathcal{E}_2$  reached zero.

However, judging from the calculation in Table 6, it was unconservative when  $k=1.00$ , giving the average accuracy (ratio between experimental and calculated values in each specimen) of 0.43. It is because the boundary of the strut is not reasonable, where  $\mathcal{E}_2$  reached zero. Moreover, the distribution of  $\mathcal{E}_2$  is not uniform in the section. However, the uniform distribution was assumed in this calculation. Hence, the compressive stress and the width of compressive strut should be reduced using a reduction factor from the estimation by Eq. 2. The accuracy was checked and the reduction factor,  $k$  was proposed to be 0.43 in all the cases.

To show the validity of the proposed method, the calculation of the shear capacity by the proposed method was compared with the existing methods. The existing methods were selected from the existing studies that proposed an equation for the shear capacity of RSF short beams. Equation 3 (Khuntia et al., 1999) shows an existing equation for the calculation of the shear capacity which accounts the effect of steel fibers. This equation was chosen, because the effect of shear span ratio was included in the formulation. By considering the arch action of compressive strut, the equation is applicable for short beams:

$$V_{\text{Khu}} = \left[ (0.167\alpha + 0.25F) \sqrt{f_c'} \right] b_w d, \quad (3)$$

where  $V_{\text{Khu}}$  is the shear capacity (N),  $\alpha$  is the arch action factor ( $\alpha = 2.5d/a < 3$  for  $a/d < 2.5$ ; 1 for  $a/d \geq 2.5$ ),  $F$  is the

**Table 6** Accuracy of shear capacity calculation by different equations

No.	Volume fraction (%)	$f'_c$ (MPa)	$a/d$	$b_w$ (mm)	$\theta$ (°)	$V_{exp}$ (kN)	$w$ (mm)	$V_{exp}/V_{DIC}$ ( $k=1.00$ )	$V_{exp}/V_{DIC}$ ( $k=0.43$ )	$V_{exp}/V_{Khu}$	$V_{exp}/V_{Sha}$
1	0.5	41.0	1.0	150	45	297.4	142	0.48	1.12	2.48	1.33
2			1.5		34	224.8	147 <sup>a</sup>	0.45	1.04	2.60	1.28
3			2.0		27	149.0	117	0.46	1.08	2.14	1.13
4	1.0	52.5	1.0		45	402.8	232	0.31	0.73	2.56	1.59
5			1.5		34	276.2	156	0.41	0.94	2.31	1.35
6			2.0		27	184.8	112	0.47	1.09	1.83	1.15
Average								0.43	1.00	2.32	1.31
Coefficient of variation (CV) (%)								14.8	14.8	12.7	12.9

$f'_c$ : concrete compressive strength;  $a/d$ : shear span ratio;  $b_w$ : web thickness;  $\theta$ : angle of compressive strut;  $V_{exp}$ : experimental shear capacity;  $w$ : width of compressive strut

<sup>a</sup> Obtained at the load level of 90% of the peak load, since the data at the peak load could not be obtained

fiber factor ( $F=(L_f/D_f)p_f d_f/100$ ),  $L_f$  is the length of steel fiber (mm),  $D_f$  is the diameter of steel fiber (mm),  $p_f$  is the volume fraction of steel fiber (%).  $d_f$  is the bond factor ( $d_f=1$  for hooked or crimped steel fibers;  $2/3$  for plain or round steel fibers with normal concrete;  $3/4$  for hooked or crimped steel fibers with lightweight concrete).

Shahnewaz and Alam (2014) found that the interactions between important parameters such as shear span ratio, aspect ratio, volume fraction of steel fiber are significant. Therefore, nonlinear relationships were proposed in the equations. A simplified equation for short beams is shown in the following equation:

$$V_{Sha} = \left[ 0.2 + 0.034f'_c + 19p_w^{0.087} - 5.8(a/d)^{1/2} + 3.4p_f^{0.4} - 800(L_f/D_f)^{-1.6} - 12((a/d)p_f)^{0.05} - 197((a/d)(L_f/D_f))^{-1.4} + 105(p_f(L_f/D_f))^{-2.12} \right] b_w d, \tag{4}$$

where  $V_{Sha}$  is the shear capacity (N),  $p_w$  is the tensile reinforcement ratio (%),  $p_f$  is the volume fraction of steel fiber (%),  $L_f$  is the length of steel fiber (mm),  $D_f$  is the diameter of steel fiber (mm).

Table 6 shows the accuracy of calculation of the shear capacity from the proposed equation and the existing equations.

Totally six RSF short beams were used for the estimation of the shear capacity. Beams were fabricated with the volume fraction of steel fiber from 0.5 to 1.0% and the shear span ratio ranging from 1.0 to 2.0. The accuracy of the proposed estimation method by DIC and other equations was compared. The proposed method by DIC estimated the shear capacity more accurately, while the variation was slightly higher compared to the others. Moreover, the accuracy of Eq. 3 was significantly lower than that of Eq. 4. By observing each equation, the calculation in Eq. 3 involves arch action factor, fiber factor,

and compressive strength in a form of nonlinear equation, while Eq. 4 is also a nonlinear equation but includes an additional tensile reinforcement ratio and expresses a more complicated form. The experimental results in this research also shows that there is a correlation between the shear span ratio and the volume fraction of steel fiber. Therefore, a more complicated expression might be a solution for the calculation of the shear capacity. In addition, Eq. 4 might be more updated and based on a larger number of data.

The proposed method by DIC was able to grasp the width of compressive strut to be used for the estimation

of the shear capacity of RSF short beams, while the other equations used the effect of related parameters only, without directly considering the contribution of the compressive strut. There is still a reduction factor in the proposed equation. However, DIC was used as the tool for investigating the compressive strut for the equation. This is the significant addition in the estimation of the shear capacity.

This shows that it is very important to study and reflect the effect of the applied load on the beam directly such as the strain distribution in the beams for the estimation of the shear capacity. According to MacGregor (1997), after diagonal cracking or steel unbonding, the shear flow cannot be transmitted. The load after the interruption of shear flow was carried by arch action in the form of compressive strut which represented concrete compressive stress fields.

The compressive stress caused the concentration of the compressive strain. By capturing the strain distribution that reflected the effect of the applied load directly during the loading test, the contribution to the shear capacity was straightforwardly estimated. In this research, the contribution of the compressive strut of which width was evaluated by the strain distribution obtained from DIC and the compression force was calculated by the compressive stress in cracked concrete.

This research relies significantly on DIC for the estimation of the shear capacity of RSF short beams. However, DIC requires the knowledge and experience for the application. Moreover, there are limitations such as light sensitivity, preparation of measurement surface, loss of data points after spalling of concrete (Gencturk et al., 2014).

In this research, the aim is to estimate the width of compressive strut by DIC. From the results of DIC, the width can be estimated. The ultimate strain in compression of concrete is generally considered to be 0.0035. The results from DIC around the compressive strut were less than and more than this ultimate strain. Nevertheless, the parabolic functions estimated from DIC can be used to estimate the width of compressive strut for the estimation of the shear capacity of RSF short beams. Moreover, the strain distribution at A, B and C was corresponding to the Saint–Venant’s Principle, the strain values decreased at B and C which are distanced from the loading and supporting points. Therefore, the results of DIC is reasonable, because they were corresponding to the theory of mechanics of structure.

The details and discussions regarding DIC will be described in the following. The subset size was  $25 \times 25$  and the step was  $12 \times 12$ . The gage length was 30 mm in all cases. The virtual gage length was calculated using the gage length of 30 mm, the step, and the calibration factor for conversion between units of mm and pixels. Therefore, the strain filter size is varied in each case. The significant strain noise floor, such as due to imperfections of sprayed random pattern on specimens was not analyzed with DIC. Nevertheless, DIC in this research was conducted until near failure of specimens. The noise floor should be small compared to the strain due to loading tests. One of the causes of bias noise is the resolution of luminance differences between pixels. Furthermore, the bias noise also occurs from the movement of camera or light or the unexpected movement of a specimen unrelated to the loading test. In this research, the resolution was improved by accurately interpolating luminance values between pixels using bi-cubic interpolation. The deflections of specimens at the peak load ranged from 2.26 to 4.56 mm so movements of camera, light or specimens should be smaller than the deflection. Nevertheless, the typical pattern of bias such as stripe was not

found and the results were able to be used for the estimation of the width of compressive strut for the estimation of the shear capacity of RSF short beams. Therefore, the bias noise was significantly smaller than that of the strain due to loading tests.

The gage length was fixed as 30 mm in this research. In addition, the maximum coarse aggregate size in this research was 20 mm. In concrete, when a crack occurred, if the crack passed through coarse aggregate of 20 mm size and the gage length was 20 mm, the measured strain will be incorrect, since the coarse aggregate is a hard material. Therefore, the application of a gage length larger than the maximum coarse aggregate size is preferred. According to Koohbor et al. (2017), a smaller virtual strain gage is good for the calculation of highly localized strain magnitudes, but will give a noisier strain distribution. On the contrary, a larger virtual strain gage will smooth the strain distribution but decrease the local strain information. In addition, according to Koohbor et al. (2017), the increase in the strain filter size reduces the noise, because the virtual strain gage is increased making the data points increase. In the case of the subset size, from Pan et al. (2008), the subset size is the size of area for tracking the displacement, it is critical to the accuracy of measured displacement. The subset size should be large enough for recognition of the distinctive pattern, but comes with larger error. The main correlation parameters such as subset, step and strain filter size can be optimized through sensitivity analyses for an accurate measurement (Koohbor et al., 2017).

## 7 Conclusions

1. DIC has proven to be one of the useful instruments for identification of compressive strut in RSF short beams, and the method to estimate the width of compressive strut was proposed by utilizing the  $\mathcal{E}_2$  distribution obtained from DIC results.
2. The compressive strut is the critical factor for the estimation of the shear capacity of RSF short beams. It is crucial to study and reflect the mechanism such as the stress–strain distribution on the RSF short beams directly for an accurate estimation of the shear capacity. The contribution to the shear capacity is the compressive strut which the width was evaluated by the strain distribution obtained from DIC during the loading tests and the compression force was calculated by the cracked concrete compressive stress.

**Acknowledgements**  
Not applicable.

**Author contributions**

All authors contributed to the paper, writing, data analysis and experimental works. All authors read and approved the final manuscript.

**Authors' information**

Narawit Hemstapat—Ph.D. Candidate, Department of Civil and Environmental Engineering, Tokyo Institute of Technology, 2-12-1 Ookayama, Meguro-ku, Tokyo 152-8552, Japan.

Kazumasa Okubo—Commission Researcher, Department of Civil and Environmental Engineering, Tokyo Institute of Technology, 2-12-1 Ookayama, Meguro-ku, Tokyo 152-8552, Japan.

Junichiro Niwa—Professor Emeritus, Department of Civil and Environmental Engineering, Tokyo Institute of Technology, 2-12-1 Ookayama, Meguro-ku, Tokyo 152-8552, Japan.

Mitsuyasu Iwanami—Professor, Department of Civil and Environmental Engineering, Tokyo Institute of Technology, 2-12-1 Ookayama, Meguro-ku, Tokyo 152-8552, Japan.

**Funding**

Not applicable.

**Availability of data and materials**

The data sets used and/or analysed during the current study are available from the corresponding author on reasonable request.

**Declarations****Competing interests**

The authors declare that they have no competing interests.

Received: 26 November 2022 Accepted: 22 March 2023

Published online: 14 June 2023

**References**

- Antonius, A., Karlinasari, R., Purwanto, P., & Widhianto, A. (2020). Shear strength and deformation of steel fibre-reinforced concrete beams after fire. *Advances in Concrete Construction*, 10(2), 105–111. <https://doi.org/10.12989/acc.2020.10.2.105>
- Banthia, N., & Trottier, J. F. (1994). Concrete reinforced with deformed steel fibers, Part I: Bond-slip mechanisms. *ACI Materials Journal*, 91(5), 435–446. <https://doi.org/10.14359/4059>
- Bhosale, A. B., & Prakash, S. S. (2020). Crack propagation analysis of synthetic vs. steel vs. hybrid fibre-reinforced concrete beams using digital image correlation technique. *International Journal of Concrete Structures and Materials*, 14, 1–9. <https://doi.org/10.1186/s40069-020-00427-8>
- Birincioglu, M. I., Keskin, R. S. O., & Arslan, G. (2022). Shear strength of steel fiber reinforced concrete deep beams without stirrups. *Advances in Concrete Construction*, 13(1), 1–10. <https://doi.org/10.12989/acc.2022.13.1.001>
- Destrebecq, J. F., Toussaint, E., & Ferrier, E. (2011). Analysis of cracks and deformations in a full scale reinforced concrete beam using a digital image correlation technique. *Experimental Mechanics*, 51, 879–890. <https://doi.org/10.1007/s11340-010-9384-9>
- Gencturk, B., Hossain, K., Kapadia, A., Labib, E., & Mo, Y. L. (2014). Use of digital image correlation technique in full-scale testing of prestressed concrete structures. *Measurement*, 47, 505–515. <https://doi.org/10.1016/j.measurement.2013.09.018>
- Gunawan, D., Okubo, K., Nakamura, T., & Niwa, J. (2020). Shear capacity of RC beams based on beam and arch actions. *Journal of Advanced Concrete Technology*, 18(5), 241–255. <https://doi.org/10.3151/jact.18.241>
- Jongvivatsakul, P., Watanabe, K., Matsumoto, K., & Niwa, J. (2011). Evaluation of shear carried by steel fibers of reinforced concrete beams using tension softening curves. *Journal of Japan Society of Civil Engineers*, 67(4), 493–507. <https://doi.org/10.2208/jscejmcs.67.493>
- Kaufmann, W., Amin, A., Beck, A., & Lee, M. (2019). Shear transfer across cracks in steel fibre reinforced concrete. *Engineering Structures*, 186, 508–524. <https://doi.org/10.1016/j.engstruct.2019.02.027>
- Khuntia, M., Stojadinovic, B., & Goel, S. C. (1999). Shear strength of normal and high-strength fiber reinforced concrete beams without stirrups. *ACI Structural Journal*, 96(2), 282–289. <https://doi.org/10.14359/620>
- Koohbor, B., Ravindran, S., & Kidane, A. (2017). Experimental determination of representative volume element (RVE) size in woven composites. *Optics and Lasers in Engineering*, 90, 59–71. <https://doi.org/10.1016/j.optlaseng.2016.10.001>
- Lee, J. H., Jung, C. Y., Woo, T. R., & Cheung, J. H. (2019). Post-yielding tension stiffening of reinforced concrete members using an image analysis method with a consideration of steel ratios. *Advances in Concrete Construction*, 7(2), 117–126. <https://doi.org/10.12989/acc.2019.7.2.117>
- MacGregor, J. G. (1997). *Reinforced concrete: Mechanics & design* (3rd ed.). Prentice Hall.
- Mansouri, I., Shahheidari, F. S., Hashemi, S. M. A., & Farzampour, A. (2020). Investigation of steel fiber effects on concrete abrasion resistance. *Advances in Concrete Construction*, 9(4), 367–374. <https://doi.org/10.12989/acc.2020.9.4.367>
- Marti, P., Pfy, T., Sigrist, V., & Ulaga, T. (1999). Harmonized test procedures for steel fiber-reinforced concrete. *ACI Materials Journal*, 96(6), 676–685. <https://doi.org/10.14359/794>
- Morgese, M., Domaneschi, M., Ansari, F., Cimellaro, G. P., & Inaudi, D. (2021). Improving distributed fiber-optic sensor measures by digital image correlation: Two-stage structural health monitoring. *ACI Structural Journal*, 118(6), 91–102. <https://doi.org/10.14359/51732994>
- Nuaklong, P., Chittanurak, J., Jongvivatsakul, P., Pansuk, W., Lenwari, A., & Likitler-suang, S. (2020). Effect of hybrid polypropylene-steel fibres on strength characteristics of UHPFRC. *Advances in Concrete Construction*, 10(1), 1–11. <https://doi.org/10.12989/acc.2020.10.1.001>
- Pan, B., Xie, H., Wang, Z., Qian, K., & Wang, Z. (2008). Study on subset size selection in digital image correlation for speckle patterns. *Optics Express*, 16(10), 7037–7048. <https://doi.org/10.1364/OE.16.007037>
- Placas, A., & Regan, P. E. (1971). Shear failure of reinforced concrete beams. *ACI Journal Proceedings*, 68(10), 763–773. <https://doi.org/10.14359/15237>
- Qin, X., & Kaewunruen, S. (2022). Environment-friendly recycled steel fibre reinforced concrete. *Construction and Building Materials*, 327, 126967. <https://doi.org/10.1016/j.conbuildmat.2022.126967>
- Shahnewaz, M., & Alam, M. S. (2014). Improved shear equations for steel fiber-reinforced concrete deep and slender beams (with appendix). *ACI Structural Journal*, 111(4), 851–860. <https://doi.org/10.14359/51686736>
- Swamy, R. N., & Mangat, P. S. (1974). A theory for the flexural strength of steel fiber reinforced concrete. *Cement and Concrete Research*, 4(2), 313–325. [https://doi.org/10.1016/0008-8846\(74\)90142-2](https://doi.org/10.1016/0008-8846(74)90142-2)
- Tahenni, T., Chemrouk, M., & Lecompte, T. (2016). Effect of steel fibers on the shear behavior of high strength concrete beams. *Construction and Building Materials*, 105, 14–28. <https://doi.org/10.1016/j.conbuildmat.2015.12.010>
- Tan, K. H., Murugappan, K., & Paramasivam, P. (1993). Shear behavior of steel fiber reinforced concrete beams. *ACI Structural Journal*, 90(1), 3–11. <https://doi.org/10.14359/9646>
- Vecchio, F. J., & Collins, M. P. (1986). The modified compression-field theory for reinforced concrete elements subjected to shear. *ACI Journal Proceedings*, 83(2), 219–231. <https://doi.org/10.14359/10416>
- Zarrinpour, M. R., & Chao, S. H. (2017). Shear strength enhancement mechanisms of steel fiber-reinforced concrete slender beams. *ACI Structural Journal*, 114(3), 729–742. <https://doi.org/10.14359/51689449>

**Publisher's Note**

Springer Nature remains neutral with regard to jurisdictional claims in published maps and institutional affiliations.